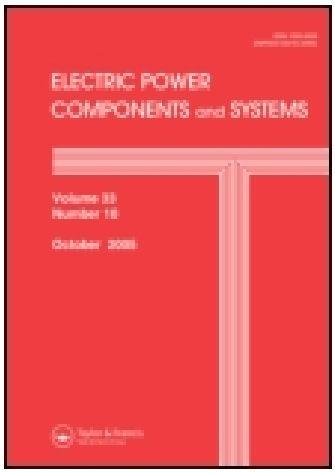

Electric Power Components and Systems
Publication details, including instructions for authors and subscription information:
http://www.tandfonline.com/loi/uemp20

Identification of the Critical Characteristics of Different Types of Voltage Sags for Synchronous Machine Torque Oscillations

Jaber Alipoor[a], Aref Doroudi[b] & Seyed Hossein Hosseinian[c]
[a] Division of Electrical, Electronic and Information Engineering, Graduate School of Engineering, Osaka University, Osaka, Japan
[b] Department of Electrical Engineering, Shahed University, Tehran, Iran
[c] Department of Electrical Engineering, Amirkabir University of Technology, Tehran, Iran
Published online: 09 Sep 2014.

To cite this article: Jaber Alipoor, Aref Doroudi & Seyed Hossein Hosseinian (2014) Identification of the Critical Characteristics of Different Types of Voltage Sags for Synchronous Machine Torque Oscillations, Electric Power Components and Systems, 42:13, 1347-1355

To link to this article: http://dx.doi.org/10.1080/15325008.2014.933376

Electric Power Components and Systems, 42(13):1347–1355, 2014

ISSN: 1532-5008 print / 1532-5016 online
DOI: 10.1080/15325008.2014.933376

Taylor & Francis
Taylor & Francis Group

Identification of the Critical Characteristics of Different Types of Voltage Sags for Synchronous Machine Torque Oscillations

Jaber Alipoor,[1] Aref Doroudi,[2] and Seyed Hossein Hosseinian[3]
[1]Division of Electrical, Electronic and Information Engineering, Graduate School of Engineering, Osaka University, Osaka, Japan
[2]Department of Electrical Engineering, Shahed University, Tehran, Iran
[3]Department of Electrical Engineering, Amirkabir University of Technology, Tehran, Iran

CONTENTS

Abstract—This article investigates the effects of symmetrical and unsymmetrical voltage sags on an important characteristic of torque pulsation of synchronous machines. Voltage sags may cause high torque pulsations, which can damage the shaft or equipment connected to it. Duration, magnitude,and initial point-on-wave of the voltage sag are the major characteristics that can influence the synchronous motors torque transients. The effect of the characteristics on the severity of the transient torque is clarified parametrically, and the critical characteristics of each type of voltage sag are extracted. A theoretical analysis is first presented to determine the severest conditions. In this analysis, for each type of voltage sag, the stator flux trajectory in complex coordination is traced to monitor its variation during and after sag. By this method, the effects of different sag types can easily be compared during the sag and at the sag ending instant. To justify the theoretical analysis, simulations of a typical synchronous motor are carried out that confirm the theoretical analysis.

1. INTRODUCTION

Voltage sags (dips) are one of the most frequent phenomena in power systems. The definition of voltage sag is a momentary reduction (10 to 90%) in the RMS of supply voltage, which lasts from half a cycle at power supply frequency to 1 min [1–3]. Voltage sags are so common for the essence of their originators that are faults in power systems and starting large loads [4–7]. In brief, when a fault occurs in a power line, consumers on all other feeders that feed from a common bus with a faulted line observe voltage sag.

If an electrical machine is subjected to voltage sags, high torque peaks may develop [8–10]. In the case of synchronous machines, these torque pulsations may pull the motor out of step or damage the motor shaft or equipment connected to it. To inhibit these conditions, protection equipment disconnects the motor from the supply. On the other hand, in some

Keywords: flux trajectory, power quality, synchronous machines, torque oscillations, voltage sag, voltage dip
Received 9 January 2013; accepted 7 June 2014
Address correspondence to Mr. Jaber Alipoor, Division of Electrical, Electronic and Information Engineering, Graduate School of Engineering, Osaka University, 2-1 Yamada-oka, Suita, Osaka 565-0871, Japan. E-mail: alipoor@pe.eei.eng.osaka-u.ac.jp
Color versions of one or more of the figures in the article can be found online at www.tandfonline.com/uemp.

applications, the continuity and smoothness of the process is important. By tuning the settings of the protection devices, dispensable disconnections can be avoided. In these cases, the torque pulsation severity should be evaluated to recognize the sags on which the motor can ride.

In [11], the authors modeled a synchronous machine considering different conditions of saturation. Due to saturation, the transient torque peak decreases slightly. However, the critical duration of symmetrical voltage sags is illustrated only by simulation without any illustration of critical characteristics of voltage sags by mathematical equations. Recently, the effects of symmetrical and unsymmetrical voltage sags on synchronous machine stability, concerning the part of voltage sag characteristics only by simulations of three typical synchronous machines, were addressed [12].

In this article, in both theoretical analysis and simulation, the saturation effect is not included, since the exact magnitudes of flux and torque oscillations are not intended to be estimated. But these quantities for different sag types could be compared. The main point of this article is that the mathematical equation of a state variable of machine (flux), including the voltage sag characteristics parameters, is extracted for different voltage sags types. Using these equations, the critical voltage sags specifications could be concluded easily. First, a qualitative method called "stator flux trajectory analysis" is presented to show the phenomenon occurring in a synchronous motor during voltage sags. In the proposed method, stator flux changes are analyzed in two axial complex coordinates, and severities of torque transients are estimated. The method gives the critical sags, and the severity of the sag types can be compared with each other. Second, simulations are performed on a typical synchronous motor in MATLAB/Simulink software (The MathWorks, Natick, Massachusetts, USA), and different types of voltage sags are applied to the motor to justify the proposed method.

This article is organized as follows. Sections 2 and 3 present the voltage sag classifications and their general equations in *d-q* axial coordination. To estimate the torque peak pulsations, the theoretical analysis is given in Section 4. Section 5 presents simulation results, and finally, Section 6 draws the conclusion.

2. SAG TYPES AND CLASSIFICATION

Severity of voltage sag effects on equipment depends on its specifications. Sag magnitude and duration are major specifications. In this study, it is assumed that the implemented sags are rectangular. In addition, it is assumed that the sag type does not change when the faults are cleared [13]. Voltage sags can be either symmetrical or unsymmetrical. If the individual phase voltages are equal and the phase angle relationship is 120°, the sag is symmetrical; otherwise, the ssag is unsymmetrical. A three-phase short circuit or starting of a large load can produce symmetrical sags. For symmetrical sags, the magnitude of sag is the remaining RMS voltage in per unit or the percent of rated voltage expressed by s. On the other hand, single-phase-to-ground and phase-to-phase faults cause unsymmetrical sags. Unsymmetrical sags can be divided into different types based on the difference in phase voltage magnitude and/or phase angle between them. For unsymmetrical sags, s is a coefficient that appears in voltage equations and causes a difference in their magnitude and/or phase angles. For both symmetrical and unsymmetrical sags, sag duration is the time interval between sag beginning and ending.

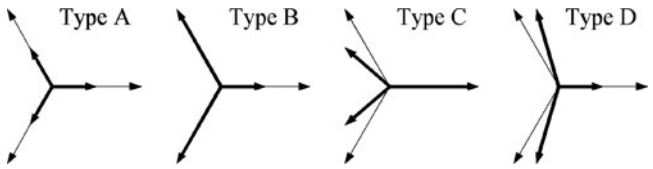

FIGURE 1. Phasor diagram of voltage sag types for $s = 0.5$.

In different references, based on the defined indices, several classifications have been done for voltage sags. The authors in [14] classified voltage sags based on fault type and transformer connections. This article deals with the main types: *A*, *B*, *C*, and *D*. Figure 1 shows their phasor diagrams for $s = 0.5$.

It should be pointed out that load and transformer connection type can change the sag type a load experiences.

3. SAGS TYPES EQUATIONS IN *d-q*-AXES COORDINATION

To apply different types of voltage sags on a synchronous machine model, the sag type voltage equation must be computed in *d-q* form (in the synchronous reference frame) using Park's transformation [15]. It is assumed that at the instant when the sag begins, the voltage of phase a is expressed by

$$v_a(t) = V_m \cos(\omega t + \theta_0). \tag{1}$$

The other phases should modify by ±120 shifting. θ_0 is the voltage phase angle at the sag beginning instant. By applying Park's transformation, symmetrical sag equations will be as follows:

$$Type\,\mathrm{A} \begin{cases} v_q(t) = sV_m \cos\theta_0 \\ v_d(t) = -sV_m \sin\theta_0 \\ v_0(t) = 0 \end{cases}, \tag{2}$$

and for unsymmetrical sags,

$$\begin{cases} v_q(t) = \frac{V_m}{3}X(s)\cos\theta_0\cos 2\omega t \\ \qquad +\frac{V_m}{3}X(s)(-\sin\theta_0)\sin 2\omega t + \frac{V_m}{3}Y(s)\cos\theta_0 \\ v_d(t) = \frac{V_m}{3}X(s)\cos\theta_0\sin 2\omega t \\ \qquad +\frac{V_m}{3}X(s)\sin\theta_0\cos 2\omega t + \frac{V_m}{3}Y(s)(-\sin\theta_0) \\ v_0(t) = \frac{V_m}{3}Z(s)\cos(\omega t + \theta_0) \end{cases}; \quad (3)$$

$X(s)$ and $Y(s)$ are functions of s such that their equations for different sag types are as follows:

$$\text{TypeB}: \begin{cases} X(s) = s-1 \\ Y(s) = s+2 \\ Z(s) = s-1 \end{cases}, \quad (4)$$

$$\text{TypeC}: \begin{cases} X(s) = \frac{3}{2}(1-s) \\ Y(s) = \frac{3}{2}(1+s) \\ Z(s) = 0 \end{cases}, \quad (5)$$

$$\text{TypeD}: \begin{cases} X(s) = \frac{3}{2}(s-1) \\ Y(s) = \frac{3}{2}(s+1) \\ Z(s) = 0 \end{cases}. \quad (6)$$

The voltage equations in d-q coordination make clear that for unsymmetrical sags, sinusoidal terms with double frequency will appear; these terms affect torque pulsations, as shown later.

4. THEORETICAL ANALYSIS

In this section, a simplified theoretical analysis is performed to obtain a qualitative understanding of the phenomena occurring in a synchronous motor during symmetrical and unsymmetrical sags. In the analysis, the flux variations are calculated in a complex plane (with d and q as axes) using the voltage sag equations. For simplicity, the stator resistance and saturation are neglected and rotor speed is assumed constant during the entire duration of the sag. As a general form, the symmetrical and unsymmetrical sags equations are different; therefore, the analysis is divided into two separate sections.

4.1. Symmetrical Voltage Sag (Type A)

Prior to the sag and in a complex plane with d- and q-axes as coordinates, the internal voltage of the machine in the synchronous reference frame can be expressed as

$$E_s = jV_m e^{j(\theta_0+\delta)}. \quad (7)$$

The synchronous reference frame is assumed to lead the stator reference frame by angle γ. Consequently, the internal voltage of the machine in the stator reference frame is given by

$$E_s^s = jV_m e^{j(\theta_0+\delta)}e^{j(\omega t+\gamma)}, \quad (8)$$

where superscript s denotes the stator reference frame. The modulus of the stator flux linkage prior to the sag is $\psi_{s0} = \frac{V_m}{\omega}$. The stator flux in stator reference frame is thus expressed as

$$\psi_s^s = \psi_d^s + j\psi_q^s = \psi_{s0}e^{j(\delta+\gamma)}e^{j(\omega t+\theta_0)}. \quad (9)$$

The sag occurs at $t = 0$. The initial fluxes in the synchronous and stator reference frames are then

$$\psi_{s(t=0)} = \frac{V_m}{\omega}e^{j(\delta+\theta_0)}, \quad (10)$$

$$\psi_{s(t=0)}^s = \frac{V_m}{\omega}e^{j(\delta+\theta_0+\gamma)}. \quad (11)$$

During the sag, the internal voltage of the machine can be given by

$$E_{s(dur.sag)}^s = jsV_m e^{j(\theta_0+\delta)}e^{j(\omega t+\gamma)}. \quad (12)$$

The change in the flux can be obtained by integration of the voltage wave:

$$\Delta\psi_{s(dur.sag)}^s = \int_0^t E_s^s dt = \frac{sV_m}{\omega}e^{j(\theta_0+\delta+\gamma)}(e^{j\omega t}-1). \quad (13)$$

The resulting flux is thus obtained by adding the change to the initial value. This results in Eq. (14):

$$\psi_{s(dur.sag)}^s = \frac{V_m}{\omega}e^{j(\theta_0+\delta+\gamma)}(1-s) + \frac{sV_m}{\omega}e^{j(\theta_0+\delta+\gamma)}e^{j\omega t}. \quad (14)$$

To find the stator flux in the synchronous reference frame, transformation coefficient $e^{-j(\omega t+\gamma)}$ can be used:

$$\psi_{s(dur.sag)} = \frac{V_m}{\omega}e^{j(\theta_0+\delta)}\left(s+(1-s)e^{-j\omega t}\right). \quad (15)$$

Equation (15) is described by a constant term and a rotating term in the negative direction. The constant term is multiplied by s, which shows the average value of flux reductions during the sag. The rotating term causes flux changes in d-q-axes coordination and, according to Eq. (16), leads to a rise in torque pulsations [8]:

$$T_e = \frac{3P}{4\omega_b}\left(\psi_d I_q - \psi_q I_d\right),$$
$$T_e = \frac{3P}{4\omega_b}\left(\frac{\psi_s\psi_{df}}{L_d}\sin\delta + \psi_s^2\left(\frac{1}{L_q}-\frac{1}{L_d}\right)\sin 2\delta\right). \quad (16)$$

According to Eq. (15) and for specified values of θ_0 and δ, the flux path during the sag will follow a circle and moves one turn in each cycle. The starting point is initial flux point. The center of the circle is the point where if the sag duration lasts enough, the flux will reach it ($\psi_{s(t=\infty)} = s\psi_{s(t=0)}$). The radius of the circle initially will be the distance between initial flux and $\psi_{s(t=\infty)}$, named ρ_d^A, and then reduces

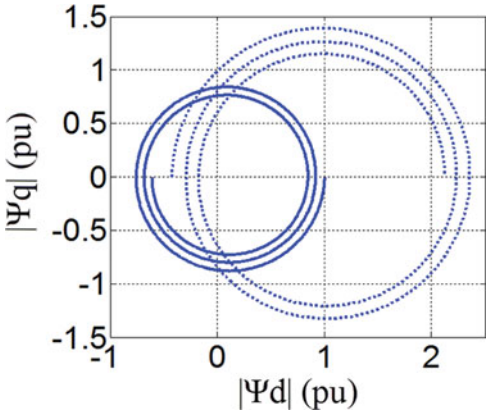

FIGURE 2. Flux path for sag type A, 10% sag of duration 2.5 cycles during (solid line) and after the sag (dashed line).

with armature time constant. During the sag, the severity of torque pulsations depends on this radius. The bigger radius of the circle is, the severer the torque pulsations are:

$$\rho_d^A = \frac{V_m}{\omega}(1-s). \tag{17}$$

Figure 2 shows the flux path (solid line) according to Eq. (15) for $s = 0.1$, $\theta_0 = 0$, and $\delta = 30^\circ$. Duration of the sag is assumed to be 2.5 cycles ($\omega t = 5\pi$). The exponential decay of the modulus is not, however, predicted by the simplified theory, as the stator resistance was neglected. Note that the radius of the circle only depends on s and is independent of θ_0 and δ.

When the voltage is restored, the flux at each point tends to go back to the initial point. Again, the flux will point along a new circle. The larger the distance is between flux at the instant of voltage restoration and initial flux, the bigger the new circle radius and the severer the torque pulsations are.

If the duration of voltage sag is a multiple of the period-time of the supply ($\omega t = 2k\pi$, where k is an integer), the stator flux will be

$$\psi_s^s = \frac{V_m}{\omega} e^{j(\theta_0+\delta+\gamma)}, \tag{18}$$

which is the same as the initial flux. This means that no additional transients would occur if the voltage was restored at that instant. On the other hand, if the duration of the voltage sag is assumed as α plus any number of full periods,

$$\psi^s_{s(t=t_{sag})} = \frac{V_m}{\omega}\left(1 - s + se^{j(\alpha+2k\pi)}\right). \tag{19}$$

When the voltage is restored, the internal voltage of the motor will be given by

$$E_s^s = jV_m e^{j(\theta_0+\delta)} e^{j(\omega t+\gamma)}. \tag{20}$$

The flux change is thus equal to

$$\begin{aligned}\Delta\psi^s_{s(aftersag)} &= \int_{t=\frac{\alpha}{\omega}}^{t} E_s^s dt \\ &= \frac{V_m}{\omega} e^{j(\theta_0+\delta+\gamma)}\left(e^{j\omega t} - e^{j\alpha}\right),\end{aligned} \tag{21}$$

and the resultant flux is

$$\psi^s_{s(aftersag)} = \frac{V_m}{\omega} e^{j(\theta_0+\delta+\gamma)}\left[(1-s)\left(1-e^{j\alpha}\right)+1\right]. \tag{22}$$

Performing the transformation in the synchronous reference frame yields

$$\psi_{s(aftersag)} = \frac{V_m}{\omega} e^{j(\theta_0+\delta)}\left[1+(1-s)\left(1-e^{j\alpha}\right)e^{-j\omega t}\right]. \tag{23}$$

This equation is similar to the expression for the stator flux during the sag in Eq. (15). An important difference is the rotating term amplitude, which is equal to the new circle radius ρ_r^A:

$$\rho_r^A = \left|(1-s)(1-e^{j\alpha})\right| = 2(1-s)\sin\frac{\alpha}{2}. \tag{24}$$

Note that the new circle radius is again independent of θ_0 and δ. The point corresponds to the maximum value of ρ_r^A, *i.e.*, $\alpha = 2k\pi + \pi$, and produces the severest torque pulsations (called critical symmetrical sag). In this situation, the flux at the ending of the sag has the maximum distance from the initial value, and the torque pulsations after the voltage restoration are maximal. Figure 2 shows the flux path (dashed line) according to Eq. (23). As seen, the new circle radius is two times ρ_d^A. Obviously, in real machines, the flux cannot reach to this level due to saturation. But by such analysis, one can find out the severity of sag with these specifications. Another interesting point is $\alpha = 2k\pi + \frac{\pi}{3}$. In this condition, $\rho_d^A = \rho_r^A$ that means the severity of torque pulsations at the sag beginning and ending are equal.

4.2. Unsymmetrical Voltage Sags

In this section, the theoretical analysis is generalized for the unsymmetrical sags. According to Eq. (3), the internal voltage in the synchronous reference frame can be written as

$$E_{s(dur.sag)} = j\frac{V_m}{3}Y(s)e^{j(\theta_0+\delta)} + j\frac{V_m}{3}X(s)e^{j(-\theta_0+\delta)}e^{-j2\omega t}. \tag{25}$$

In the stator reference frame, this voltage is given by

$$\begin{aligned}E^s_{s(dur.sag)} &= j\frac{V_m}{3}Y(s)e^{j(\theta_0+\delta+\omega t+\gamma)} \\ &\quad + j\frac{V_m}{3}X(s)e^{j(-\theta_0+\delta)}e^{-j(\omega t-\gamma)}.\end{aligned} \tag{26}$$

The flux change can be obtained by integrating the voltage during the sag:

$$\Delta\psi^s_{s(dur.sag)} = \int_0^t E^s_s dt = \frac{V_m}{3\omega} Y(s) e^{j(\theta_0+\delta+\gamma)}(e^{j\omega t} - 1) - \frac{V_m}{3\omega} X(s) e^{-j(\theta_0-\delta-\gamma)}(e^{-j\omega t} - 1). \quad (27)$$

The resulting flux is thus obtained by adding the changes to the initial value:

$$\psi^s_{s(dur.sag)} = \psi^s_{s0} + \Delta\psi^s_s = \frac{V_m}{\omega} e^{j(\theta_0+\delta+\gamma)} + \frac{V_m}{3\omega} Y(s) e^{j(\theta_0+\delta+\gamma)}(e^{j\omega t} - 1) - \frac{V_m}{3\omega} X(s) e^{-j(\theta_0-\delta-\gamma)}(e^{-j\omega t} - 1). \quad (28)$$

The flux in the synchronous reference frame will then be as follows:

$$\psi_{s(dur.sag)} = \frac{V_m}{3\omega} Y(s) e^{j(\theta_0+\delta)} + \frac{V_m}{3\omega}(3e^{j(\theta_0+\delta)} - Y(s)e^{j(\theta_0+\delta)} + X(s)e^{-j(\theta_0-\delta)})e^{-j\omega t} - \frac{V_m}{3\omega} X(s) e^{-j(\theta_0-\delta)} e^{-j2\omega t}. \quad (29)$$

Equation (29) indicates that stator flux in the synchronous reference frame consists of one constant term and two rotating terms. The velocity of one of the rotating terms is twice that of the other one.

For different sag types, by substituting $X(s)$ and $Y(s)$ from Eq. (5) and rearranging them gives

$$\text{Type B: } \psi_{s(dur.sag)} = \frac{V_m}{3\omega} e^{j\delta} \left[(s+2)e^{j\theta_0} + 2(1-s) j \sin\theta_0 e^{-j\omega t} + (1-s)e^{-j\theta_0} e^{-j2\omega t} \right], \quad (30)$$

$$\text{Type C: } \psi_{s(dur.sag)} = \frac{V_m}{2\omega} e^{j\delta} \left[(s+1)e^{j\theta_0} + 2(1-s)\cos\theta_0 e^{-j\omega t} - (1-s)e^{-j\theta_0} e^{-j2\omega t} \right], \quad (31)$$

$$\text{Type D: } \psi_{s(dur.sag)} = \frac{V_m}{2\omega} e^{j\delta} \left[(s+1)e^{j\theta_0} + 2(1-s) j \sin\theta_0 e^{-j\omega t} + (1-s)e^{-j\theta_0} e^{-j2\omega t} \right]. \quad (32)$$

Note that unlike symmetrical sags, the initial point of a wave is a parameter that can influence the flux changes. As an example, Figure 3 shows the flux path (solid line) according to Eqs. (30)–(32) for sag types B, C, and D of magnitude $s = 0.5$, duration of 5.5 cycles, $\theta_0 = 30°$, and $\delta = 0°$. Note that unlike symmetrical sags, the flux trajectory is not a circle and depends on the constant and rotating terms coefficients.

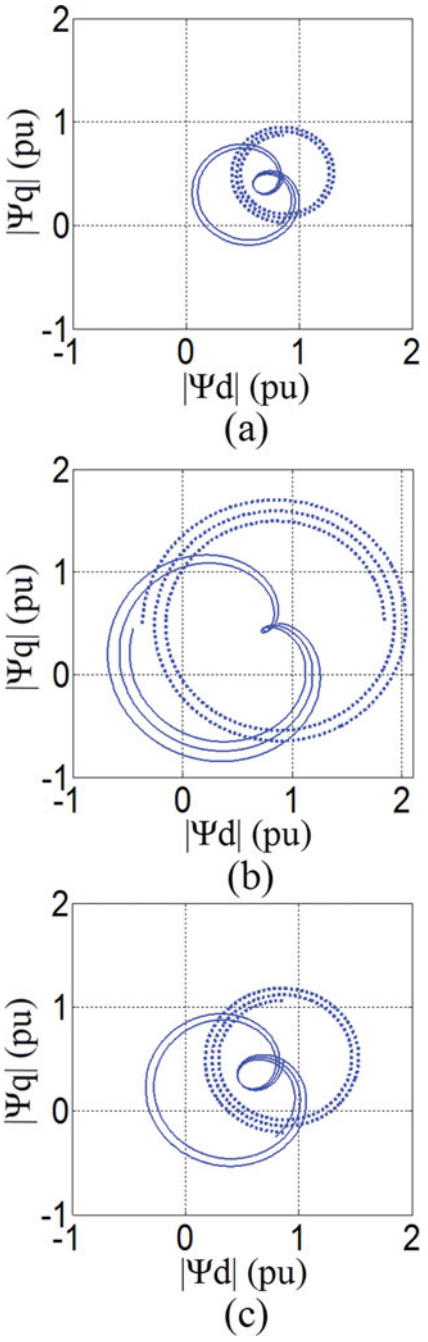

FIGURE 3. Flux trajectory during (solid line) and after (dashed line) sags of magnitude $s = 0.5$, duration 5.5 cycles, and initial point-on-wave 30°: (a) type B, (b) type C, and (c) type D.

Equations (30)–(32) are too intricate, which can be used for comparison of sag severity and specifying the most unfavorable initial point-on-wave. Therefore, the equations were written in polar coordinates (ρ and θ). By this conversion, one can easily determine the critical sags. Furthermore, sags

severity comparison can be performed by a simple parameter. A typical example of this conversion is given in Appendix A;

$$\rho_d^B = \frac{2V_m}{3\omega}(1-s)\left[\sin\theta_0 - \cos(\theta_0-\theta)\right], \tag{33}$$

$$\rho_d^C = \frac{V_m}{\omega}(1-s)\left[\cos\theta_0 - \cos(\theta_0-\theta)\right], \tag{34}$$

$$\rho_d^D = \frac{V_m}{\omega}(1-s)\left[\sin\theta_0 - \cos(\theta_0-\theta)\right]. \tag{35}$$

It is clear that the maximum ρ for sag types B and D is obtained when the initial point-on-wave is an odd multiple of 90° ($v_a(t)$ is crossing zero), while the maximum is obtained for sag type C when θ_0 is equal to an even multiple of 90° ($v_a(t)$ is extremum). On the other hand, knowing the initial point-on-wave, the equations allow a clearer comparison of the severity of the different sag types at sag beginning instant. In fact, during the sag, severity of torque pulsations depends on radius ρ_d. The bigger the radius is, the severer the torque pulsations are.

After voltage restoration, the flux points along a circle. The radius of the circle can be obtained by the following steps:

- set ωt equal to $\alpha + 2k\pi$ in Eq. (28) and compute $\psi^s_{s(t=t_{sag})}$;
- compute $\psi^s_{s(aftersag)} = \psi^s_{s(t=t_{sag})} + \Delta\psi^s_s$; $\Delta\psi^s_s$ can be obtained from Eq. (21);
- determine $\psi_{s(aftersag)} = \psi^s_{s(aftersag)} e^{-j(\omega t+\gamma)}$.

The result is given as follows:

$$\psi_{s(after.sag)} = \frac{V_m}{3\omega}e^{j\delta}\left[3e^{j\theta_0} + \left[(3-Y(s))(1-e^{j\alpha})e^{j\theta_0} + X(s)(1-e^{-j\alpha})e^{-j\theta_0}\right]e^{-j\omega t}\right]. \tag{36}$$

Equation (36) shows that if the duration of unsymmetrical sags is a multiple of the period time of the supply, the stator flux will be the same as the initial flux and no additional transients would occur. For other durations ($\omega t = \alpha + 2k\pi$), the radius of the circle is obtained by the following equations:

$$\rho_r^B = \frac{4V_m}{3\omega}(1-s)\sin\frac{\alpha}{2}\cos\left(\theta_0+\frac{\alpha}{2}\right), \tag{37}$$

$$\rho_r^C = \frac{2V_m}{\omega}(1-s)\sin\frac{\alpha}{2}\sin\left(\theta_0+\frac{\alpha}{2}\right), \tag{38}$$

$$\rho_r^D = \frac{2V_m}{\omega}(1-s)\sin\frac{\alpha}{2}\cos\left(\theta_0+\frac{\alpha}{2}\right). \tag{39}$$

Figure 3 shows the flux path (dashed line) according to Eqs. (37)–(39) for sag types B, C, and D. Equations (37)–(39) show that at the voltage restoration instant, higher torque peaks are produced when the sag duration is half a period plus any number of full periods. Thus, the critical sags are produced in the following conditions:

Types B and D: $\theta_0 = 90^\circ$, $\omega t = 2k\pi + \pi$;
Type C: $\theta_0 = 0^\circ$, $\omega t = 2k\pi + \pi$.

Comparison of the sag types at the sag beginning and ending can be also carried out by the two parameters ρ_d and ρ_r.

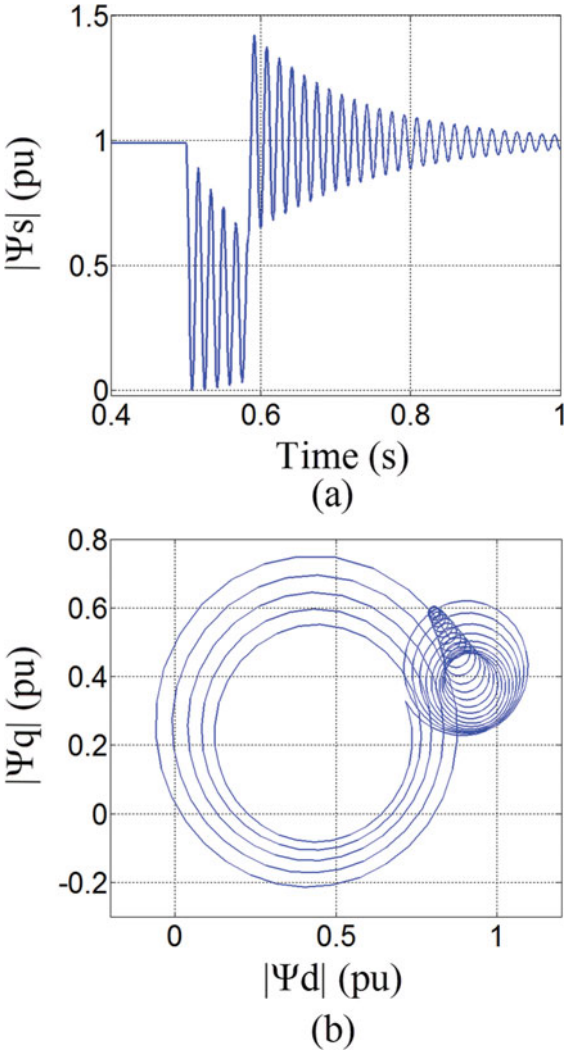

FIGURE 4. (a) Stator flux magnitude versus time and (b) stator flux in complex coordination in the synchronous reference frame during and after a symmetrical sag of amplitude $s = 0.5$ and duration of five cycles.

5. SIMULATIONS

To justify the theoretical analysis, a salient-pole 4150-kVA synchronous machine is modeled using the generalized Park's model [15] in MATLAB/Simulink based on [16]. The machine has one damper winding in the d-direction and one in the

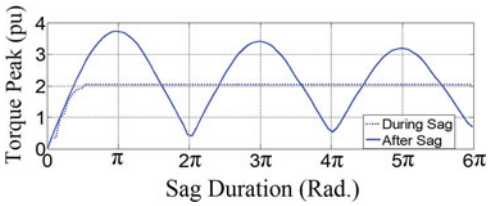

FIGURE 5. Torque peaks during (dashed line) and after (solid line) symmetrical voltage sag versus sag duration for symmetrical sag.

q-direction. The machine mathematical model details can be found in [15]. The motor parameters and rated quantities are given in Appendix B.

Before voltage sag, the motor draws 1 p.u. of real power in nominal terminal voltage and at unity power factor. During voltage sag, load torque and excitation voltage are assumed to be constant.

Figure 4 shows stator flux in the synchronous reference frame during and after a symmetrical voltage sag of amplitude $s = 0.5$ and a duration of five cycles occurs at motor terminals.

As expected, during the sag, the flux has followed a circle and, after voltage restoration, pointed along a new circle. Since the sag duration is a multiple of the period time of the supply, at the voltage restoration instant, the flux is close to its initial position, and hence, the severity of torque pulsations is minimal.

Figure 5 shows the torque peaks after the sag ending as a function of voltage sag duration. For comparison, the torque peak at sag beginning is also presented ($s = 0.5$). As seen, there is a sinusoidal-like dependency to the sag duration. The

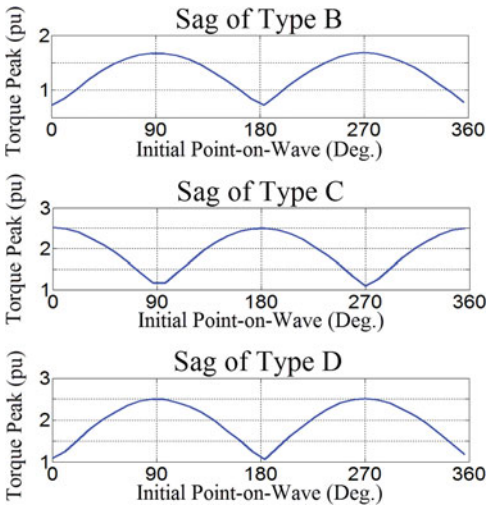

FIGURE 6. Torque peaks during the sag for different unsymmetrical sag types versus initial point-on-wave.

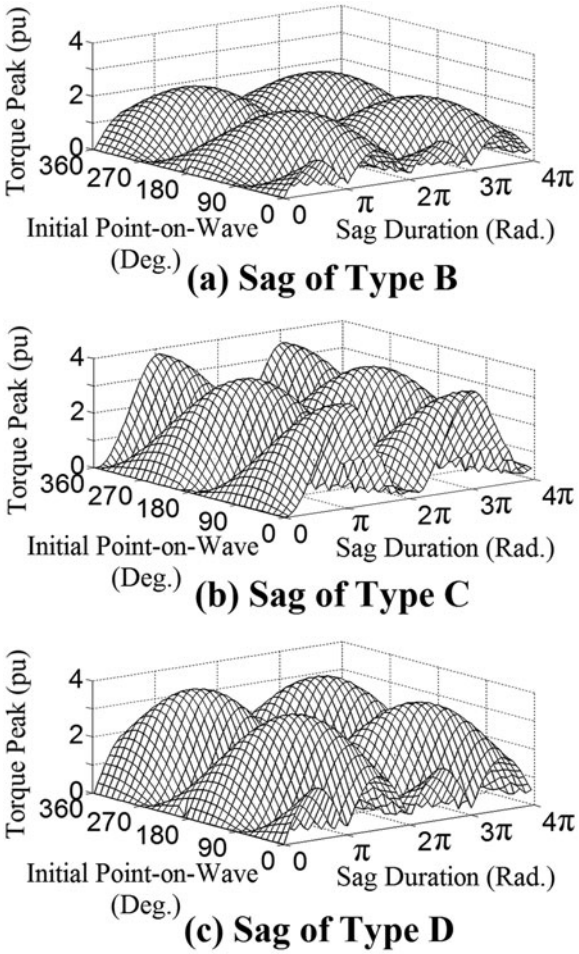

FIGURE 7. Torque peaks at the sag ending for different unsymmetrical sag types versus initial point-on-wave and sag duration.

worst case is clearly voltage sag lasting on half a cycle, where the torque peak is about 3.7 p.u.

As mentioned, for unsymmetrical sags, the torque peak at the sag beginning is affected by the initial point-on-wave and sag depth. Figure 6 shows the torque peaks versus θ_0 for different unsymmetrical sag types of amplitude $s = 0.5$. The points correspond to the torque pulsations peak can easily be obtained from this figure.

At the sag ending, the torque peaks also depend on the duration of the sag. Figure 7 shows the three-dimensional surfaces of the torque peaks versus θ_0 and ωt for sag types B, C, and D.

The figure depicts that the critical sags are as follows:

Types B and D: $\theta_0 = 90^\circ$, $\omega t = 2k\pi + \pi$,
Type C: $\theta_0 = 0^\circ$, $\omega t = 2k\pi + \pi$,

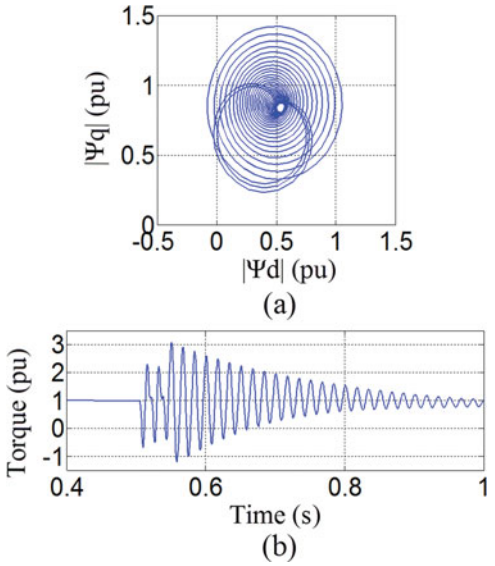

FIGURE 8. (a) Stator flux in complex plane in the synchronous reference frame and (b) electromagnetic torque of the motor subjected to sag type B of duration 2.5 cycles and initial point-on-wave 90°.

which are the same as the values predicted by the theoretical analysis. Finally, Figure 8 shows flux and torque at the critical conditions for unsymmetrical sag type B ($s = 0.5$).

6. CONCLUSION

A simplified theoretical analysis is presented to investigate the effects of different types of voltage sags on synchronous motors torque pulsations. The method can easily specify the most unfavorable conditions during and at the ending instant of the different sags types. During a sag, the effects of symmetrical sags depend on the depth of the sag, while for unsymmetrical sags, the initial point-on-wave and depth of the sag can influence the synchronous motor torque peaks. For sag types B and D, initial point-on-waves of an odd multiple of 90° have the severest torque transients, while for the sag type C, initial point-on-waves of an even multiple of 90° have the severest torque transients. At the voltage restoration instant, for both symmetrical and unsymmetrical sags, when unsymmetrical sags have their worst condition for initial point-on-wave, the maximum torque peaks occur when the sag duration equals multiples of a full period of the supply plus half a cycle. The proposed theoretical method can also be applied to compare the effects of different sag types on the torque peaks. To justify the theoretical analysis, simulations were performed, and the results show the accuracy of the proposed method. By identifying the critical voltage sags, sags that produce hazardous torque oscillations could be prevented from reaching the motor. Also, machines can be made more robust by design and tests carried out for and under the most severe condition. Furthermore, a fine tuning of protection system can be achieved to avoid unnecessary outages.

REFERENCES

[1] Kennedy, B. W., "Power quality characteristics," *Power Quality Primer*, New York: McGraw-Hill, Chap. 2, p. 34, 2000.

[2] Dugan, R. C., McGranaghan, M. F., Santoso, S., and Beaty, H. W., "Terms and definitions," *Electrical Power Systems Quality*, 2nd ed., New York: McGraw-Hill, Chap. 2, p. 20, 2004.

[3] Sankaran, C., "Power frequency disturbance," *Power Quality*, Boca Raton, FL: CRC Press LLC, Chap. 2, 2002.

[4] IEEE, "IEEE recommended practice for monitoring electric power quality," IEEE Standard 1159–1995, 1995.

[5] Bollen, M. H. J., *IEEE Tutorial on Voltage Sag Analysis*, New York: IEEE Press, October 1999.

[6] Conrad, L. E., and Bollen, M. H. J., "Voltage sag coordination for reliable plant operation," *IEEE Trans. Industry Appl.*, Vol. 33, No. 6, pp. 1459–1464, 1997.

[7] Arrillaga, J., Bollen, M. H. J., and Watson, N. R., "Power quality following deregulation," *Proc. IEEE*, Vol. 88, No. 2, pp. 246–261, February 2000.

[8] Carlsson, F., Nee, H. P., and Sadarangani, C., "Analysis of peak torque of line-operated synchronous machines subjected to symmetrical voltage sags," *International Conference on Power Electronics, Machines and Drives*, pp. 480–485, Bath, UK, 16–18 April 2002.

[9] Das, J. C., "Effects of momentary voltage dips on the operation of induction and synchronous motors," *IEEE Trans. Industry Appl.*, Vol. 26, No. 4, pp. 711–718, 1990.

[10] Guasch, L., Córcoles, F., and Pedra, J., "Effects of symmetrical and unsymmetrical voltage sags on induction machines," *IEEE Trans. Power Delivery*, Vol. 19, No. 2, pp. 774–782, 2004.

[11] Kar, N. C., and El-Serafi, A. M., "Effect of voltage sag on the transient performance of saturated synchronous motors," *Canadian Conference on Electrical and Computer Engineering (CCECE)*, pp. 1246–1251, Ottawa, Canada, 7–10 May 2006.

[12] Aguilar, D., Rolan, A., Vazquez, G., Corcoles, F., and Rodriguez, P., "Symmetrical and unsymmetrical voltage sag effects on the three-phase synchronous machine stability," *13th European Conference on Power Electronics and Applications (EPE)*, pp. 1–7, Barcelona, Spain, 8–10 September 2009.

[13] Bollen, M. H. J., "Voltage recovery after unbalanced and balanced voltage dips in three-phase systems," *IEEE Trans. Power Delivery*, Vol. 18, No. 4, pp. 1376–1381, 2003.

[14] Dugan, R. C., McGranaghan, M. F., Santoso, S., and Beaty, H. W., "Voltage sags and interruptions," Electrical Power Systems Quality, 2nd ed., New York: McGraw-Hill, p. 53, 2004.

[15] Krause, P. C., Wasynczuk, O., and Sudhoff, S. D., "Reference frame theory," *Analysis of Electric Machinery and Drive Systems*, 2nd ed., New York: Wiley-IEEE Press, pp. 109–140, 2002.

[16] Ong, C. M., "Synchronous machines," *Dynamic Simulation of Electrical Machinery, Using Matlab/Simulink*, Upper Saddle River, NJ: Prentice Hall PTR, pp. 259–350, 1998.

[17] Carlsson, F. "Explanation to irregularities in the dependence between voltage sag magnitude and the tripping level for line operated synchronous machines," *38th IAS Ann. Mtg. Indust. Appl. Conf.*, Vol. 2, pp. 1085–1062, October 2003.

APPENDIX A

Expressing Eq. (30) in the form of $a + ib$ (real and imaginary parts) gives

$$\begin{aligned}\psi_d^B = \frac{V_m}{3\omega}e^{j\delta}[&(s+2)\cos\theta_0 + 2(1-s)\sin\theta_0\sin\omega t\\ &+(1-s)\cos\theta_0\cos 2\omega t - (1-s)\sin\theta_0\sin 2\omega t\\ &+j((s+2)\sin\theta_0 + 2(1-s)\sin\theta_0\cos\omega t\\ &-(1-s)\cos\theta_0\sin 2\omega t - (1-s)\sin\theta_0\cos 2\omega t)].\end{aligned} \tag{A1}$$

Flux components at the x- and y-directions will then be as follows:

$$\begin{aligned}\psi_x^B - 3\cos\theta_0 &= \frac{2V_m}{3\omega}e^{j\delta}(1-s)\sin\omega t\\ &\quad\times[\sin\theta_0 - \cos\theta_0\sin\omega t - \sin\theta_0\cos\omega t].\\ \psi_y^B - 3\sin\theta_0 &= \frac{2V_m}{3\omega}e^{j\delta}(1-s)\cos\omega t\\ &\quad\times[\sin\theta_0 - \cos\theta_0\sin\omega t - \sin\theta_0\cos\omega t].\end{aligned} \tag{A2}$$

By squaring and rearranging the above equations, the flux equation in polar coordinates is given by Eq. (A3):

$$\Psi_X^{B^2} + \Psi_Y^{B^2} = \left(\frac{2V_m}{3\omega}e^{j\delta}(1-s)\right)^2[\sin\theta_0 - \cos(\theta_0-\theta)]^2, \tag{A3}$$

where

$$\begin{cases}\Psi_X^B = \psi_x^B - 3\cos\theta_0\\ \Psi_Y^B = \psi_y^B - 3\sin\theta_0\\ \theta = \arctan\frac{\Psi_Y^B}{\Psi_X^B}, \theta = \omega t - \frac{\pi}{2}\end{cases}.$$

Equation (A3) has a circular form for which its radius ρ changes by θ_0 and ωt:

$$\rho_d^B = \frac{2V_m}{3\omega}(1-s)[\sin\theta_0 - \cos(\theta_0-\theta)]. \tag{A4}$$

APPENDIX B

Ratings and parameters of the 4150-kVA synchronous motor are stated in Table B1 [17].

Quantity	Symbol	Value	Unit
Speed	n	1800	r/min
Inertia	J	960	kgm^2
Voltage line–line	U_{ll}	10.5	kV
Apparent power	S	4150	kVA
Current	I	228	A
Power factor	$\cos\phi$	0.9	Capacitive
Pole pairs	P	2	—
Inductance d	L_d	151	mH
Transient inductance d	L'_d	25	mH
Subtransient inductance d	L''_d	17	mH
Inductance q	L_q	75	mH
Subtransient inductance q	L''_q	26	mH
Armature time constant	T_a	0.1	sec
Field winding time constant	T_{d0}	4.33	sec

TABLE B1. Rated data and parameters of synchronous machine.

BIOGRAPHIES

Jaber Alipoor received his B.Sc. from the Electrical Engineering Department of Mazandaran University, Iran, in 2007 and his M.Sc. from the Electrical Engineering Department of Shahed University, Tehran, Iran in 2010. At present, he is a Ph.D. student at Osaka University, Japan. His fields of interest are power quality, voltage stability analysis, and contingency ranking.

Aref Doroudi received his B.Sc. from the Electrical Engineering Department of Amirkabir University of Technology, Tehran, Iran, in 1992; his M.S. in electrical engineering from Tabriz University, Tabriz, Iran, in 1994; and his Ph.D. in electrical engineering from Amirkabir University of Technology, Tehran, Iran, in 2000. He is presently an assistant professor of the Electrical Engineering Department, Shahed University, Tehran, Iran. His fields of interest include power quality, electric machines design, and power systems dynamic.

Seyed Hossein Hosseinian received both his B.Sc. and M.Sc. from the Electrical Engineering Department of Amirkabir University of Technology, Iran, in 1985 and 1988, respectively, and his Ph.D. from the in Electrical Engineering Department, University of Newcastle, England, in 1996. He is currently an associate professor in the Electrical Engineering Department, Amirkabir University of Technology (AUT). He is the author of 4 books in the field of power systems and author/co-author of over 100 technical papers. His fields of interest include transient in power systems, power quality, restructuring, and deregulation in power systems.